PHYSICAL REVIEW B VOLUME 24, NUMBER 6 15 SEPTEMBER 1981

Surface plasmons confined by microstructures on tunnel junctions

R. W. Rendell* and D. J. Scalapino
Department of Physics, University of California, Santa Barbara, California 93106

(Received 29 January 1981)

The properties of surface plasmons excited by electron tunneling near metallic structures with dimensions of a few hundred angstroms are examined. The excitations become localized by the microstructures, and the dependence of the dominant frequencies of these localized modes on junction geometry, material, and mode type is discussed. A calculation of the excited modes for thin rod microstructures is presented within an equivalent-circuit approximation. A complete calculation is given for surface plasmons localized by particles with curvature near the junction, including the radiation spectrum of the system. A distribution of particle microstructures is examined within an effective-medium theory. Comparison with experiments is made.

I. INTRODUCTION

New technologies have been developed in the past decade for fabricating surface microstructures on the micrometer and submicrometer scale. The potential for building precision structures a few hundred angstroms in size now exists, and this will present an opportunity to study new physical phenomena associated with them.[1] In particular, the possibility arises of modifying and controlling well-known surface excitations such as surface plasmons, phonons, polaritons, and magnons. In this paper we study surface plasmons confined by microstructures on tunnel junctions.

Nonradiative surface plasmons can propagate along the smooth interface between a metal and an insulator at frequencies below the bulk-plasma frequency and above the conduction-electron relaxation frequency of the metal. The phase velocity of the modes parallel to the interface is less than that of light and, because momentum and energy cannot be simultaneously conserved at the boundary, these excitations are not coupled to free-space electromagnetic waves. Random surface irregularities, or roughness, on the metal have long been of interest because they can cause the surface plasmon to be scattered into other surface-plasmon states or radiate electromagnetic energy. Lambe and McCarthy have observed light emission from Al-metal tunnel junctions with slightly roughened counterelectrodes (roughness height typically 50 Å) made of Ag, Au, Pb, or In.[2] They demonstrated that the excited fields decay rapidly in the direction normal to the counterelectrode and that the coupling to the emitted radiation increases with roughness consistent with the behavior of surface plasmons on a surface with small-amplitude roughness.[3] McCarthy and Lambe later observed similar effects using semiconducting Sn-doped indium oxide counterelectrodes.[4]

The physics of surface plasmons on rough surfaces has usually been handled theoretically by assuming a surface roughness profile function $\xi(\vec{x}_\parallel)$ characterized by a random (often Gaussian) distribution of Fourier coefficients.[5] Parameters characterizing the surface can then be written in terms of this distribution, such as the root-mean-square deviation of the surface from flatness δ^2 [i.e., $\langle \xi^2(0)\rangle = \delta^2$] and the transverse correlation length a which gives a measure of the average distance between successive peaks and valleys on the surface [i.e., $\langle \xi(\vec{x}_\parallel)\xi(\vec{0})\rangle = \delta^2 \exp(-x_\parallel^2/a^2)$]. With use of these parameters, the surface roughness is then treated as a perturbation which scatters a surface plasmon, and the scattered electromagnetic fields in both the solid and the region outside it are calculated in a Born approximation. This perturbation approach calculates the scattered fields as if they were produced by surface currents additional to those on a smooth surface, and to a first approximation the rough surface is replaced by a smooth one with an additional layer of currents whose amplitude is proportional to the height of the roughness. The perturbation treatments are valid only when a surface-plasmon wavelength can contain many roughness peaks and valleys (i.e., the surface irregularities are rather densely packed), and when effects of the roughness structure beyond those of a smooth surface are not important.[6]

Recently experiments on light-emitting tunnel junctions utilizing roughened counterelectrodes in the form of evaporated Au particles (particle size typically 300 Å diameter) have been reported by Hansma and Broida[7] and by Adams, Wyss, and Hansma.[8] The emission spectra of these junctions is found to differ qualitatively from those of junctions with small-scale roughness used by Lambe and McCarthy. For junction bias voltages

$\gtrsim 2$ V, the emission spectrum showed a resonant structure near $\hbar\omega = 1.9$ eV. In a recent calculation by the authors and B. Mühlschlegel,[9] the physics of the large-scale roughness junctions was interpreted by introducing the concept of a localized surface plasmon. Extended surface plasmons become trapped in the manner of a waveguide beyond the cutoff formed beneath the metal particle. Localized plasmons may also play a role in the experiments of Jain, Wagner, and Olson[10] on Mg-Ag junctions where roughness on the Ag electrode was on the scale of 10^3 Å in height and the experiments of McCarthy and Lambe[4] on junctions using counterelectrodes formed by 400 Å Ag particles.

When coupling to the radiation field is neglected, the dispersion relation $\omega(q)$ of a nonradiative surface plasmon propagating between a perfectly smooth metal surface and an insulator asymptotically approaches a maximum frequency ω_{sp} as $q \to \infty$ due to polarization effects at the interface. For a free-electron metal above vacuum, $\omega_{sp} = \omega_p/\sqrt{2}$, where ω_p is the bulk-plasma frequency. We can understand the qualitative effects on the surface plasmons produced by surface irregularities by using a special form of roughness, that of a periodic line grating on the metal surface with spacing d. Two extreme approximations are useful when analyzing this situation. First, if the grating lines are very shallow, the $\omega(q)$ relationship is then similar to that of a smooth surface, and the grating is only a small perturbation so that the perturbation theories should be applicable. The effect of the grating is to produce narrow forbidden-frequency bands near $q = n\hbar\pi/d$ within an otherwise continuous variation of ω with q. Ritchie *et al.*[11] have indeed found evidence for such allowed and forbidden bands for surface plasmons on an Au surface perturbed by a diffraction line grating. Such band gaps can even appear under certain conditions on surfaces with small amplitude random roughness.[12]

A second extreme approximation is possible if the grating lines are very thick and protrude above the surface. Then the structure resembles an assembly of resonant cavities weakly coupled together. The resonant frequency of each cavity is only slightly affected by its neighbors, and only narrow allowed frequency bands, separated by wide forbidden gaps, appear. The frequencies of the allowed bands are near the resonant frequencies of the cavities. If the structure of the surface irregularities themselves could support resonances, as in the metal-particle tunnel junctions, then we would still expect these same general features even if the array of surface irregularities were nonperiodic. A set of discrete resonant cavity frequencies would lie below an upper surface-plasmon frequency limit. This upper frequency will in fact be the same limit as that found in the smooth surface case ω_{sp} because the very large wave vector modes will not feel the structure of the roughness. It is this second resonant cavity approximation in which localized surface-plasmon solutions can be found that we are concerned with in this paper.

Localized surface plasmons are expected to be excited in a variety of physical situations which involve surface microstructures, and thus an understanding of their properties and how these depend on microstructure geometry is desirable. In addition to the surface-plasmon resonant cavities formed on tunnel junctions by the random distribution of metal particles, precisely engineered surface-plasmon waveguides and cavity structures will be made available by microfabrication technology in the coming decade.[1] Localized surface plasmons are also expected to play a role in light-scattering experiments from metal foils which have large-scale roughness.[13] The localized surface-plasmon concept was found to be important in a recent theoretical study of modes associated with voids near the surface of radiation-damaged metals.[14] Experimental studies of surface-enhanced Raman scattering (SERS) in an ultrahigh vacuum[15] have shown that the enhancement is favored by roughness in the form of metal spheroids approximately 500 Å in size on the surface separated by 1500—3000 Å. The enhancement takes place for molecules positioned out to 100 Å or more from the surface. This has suggested to many workers that localized surface plasmons may play an important role in SERS. Recent theoretical studies have supported this idea.[16,17]

In Sec. II A, we discuss the qualitative dependence of the local mode frequencies on the microstructure geometry for some simple surface microstructures. Section II B examines more closely the excitation of a localized plasmon for the particular case of thin rodlike microstructures within an equivalent circuit approximation. Section III A presents a detailed calculation of tunneling excitation of plasmons confined by microstructures which have a finite curvature near the junction surface. In Sec. III B, a random surface distribution of these microstructures is examined within an effective medium theory. Section III C discusses the calculated radiation spectrum of this system and compares it to the recent metal-particle tunneling experiments[7,8] and to the recent theory of light emission from roughened junctions by Laks and Mills,[18,19] which use perturbation techniques for treating the roughness.

II. MICROSTRUCTURE EXCITATIONS

A. General features

For purposes of making some physical estimates and illustrating the basic ideas concerning the excitation of surface plasmons near surface microstructures on tunnel junctions, we consider some prototype microstructures in Figs. 1(b), 1(c), and 1(d). These can be viewed as modifications of the smooth surface tunnel junction of Fig. 1(a) in which the planar counterelectrode is replaced by either a spherical particle, a cylindrical slab, or a cylindrical rod. We assume that the bottom electrode is extremely thick. If these modified junctions are biased with a dc voltage V_0, we expect to produce excitations with energy $\lesssim eV_0$ in the vicinity of the microstructures by electron tunneling. We will first confine our attention to a single microstructure and in Sec. III B we will examine a distribution of microstructures over the junction surface.

Surface plasmons in these structures can be described classically and found as solutions of Maxwell's equations. However, we do not need to solve these exactly, as can be seen from an order-of-magnitude estimate. If we consider a plasmon field of characteristic wavelength λ_s, then Maxwell's equations imply that $H(\omega)/\epsilon(\omega)E(\omega) \sim \lambda_s/\lambda$, where $\lambda = 2\pi c/\omega$, and $H(\omega)$ and $E(\omega)$ are the Fourier components of the magnetic and electric fields, respectively. Thus for $\lambda_s/\lambda \ll 1$ the magnetic fields can be neglected. The implication is that restoring forces for oscillating surface charges of the plasmon field come from charges nearly compared to radiation wavelengths and retardation can be neglected. We will be concerned with microstructures with the largest dimensions on the order of $(2-5)\times 10^2$ Å operating at optical frequencies.

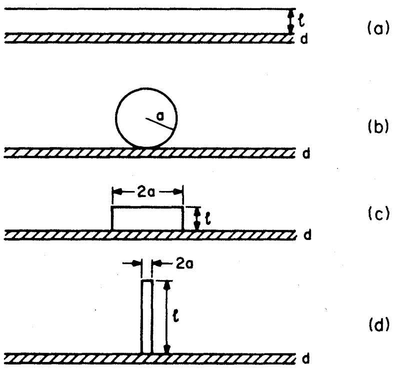

FIG. 1. Prototype microstructures on a tunnel junction. Shown are (a) a smooth metal layer, (b) a spherical particle, (c) a cylindrical slab, and (d) a cylindrical rod.

Neglecting retardation we look for a potential satisfying

$$\vec{\nabla}[\epsilon(\vec{x},\omega)\vec{\nabla}\psi] = -4\pi\rho(\vec{x},\omega) \qquad (2.1)$$

and fulfilling boundary conditions appropriate to the microstructure. The tunneling charge fluctuations $\rho(\vec{x},\omega)$ drive the surface plasmons. A form for this is obtained in Appendix A and will be needed in later sections, but at this point we make some estimates of the dispersion relations for the structures in Fig. 1. For purposes of the discussion in this section we will take the substrate and the microstructure counterelectrode to both be described by the same dielectric function $\epsilon(\omega)$, and we will take the dielectric constant of the oxide tunneling barrier and the space surrounding the microstructure to be unity.

The dispersion relation for the junction of Fig. 1(a) with the smooth planar counterelectrode is easily found by Fourier transforming the spatial dependence of the potential along the direction of the interfaces (i.e., the $\vec{r}$ direction, in cylindrical coordinates) and looking for solutions to Laplace's equation in the different regions of the form $\psi(q,z) = A\exp(-i\vec{q}\cdot\vec{r})\exp(\pm qz)$. The conditions that ψ and $\epsilon\, d\psi/dz$ be continuous at the interfaces are thus easily satisfied, and we find these conditions require the following dispersion relation:

$$0 = (\epsilon+1)\left\{\left[\epsilon\tanh\left(q\frac{d}{2}\right)+1\right]\left[\tanh\left(q\frac{d}{2}\right)+\epsilon\right] - (1-\epsilon)^2 e^{-2ql}\tanh\left(q\frac{d}{2}\right)\right\}. \qquad (2.2)$$

We now allow the junction materials to be free-electron metals, $\epsilon(\omega) = 1-(\omega_p/\omega)^2$, where ω_p is the bulk-plasma frequency, in order to get a feel for some limiting cases of this expression. The imaginary part is neglected so that the use of a single dispersion curve to discuss the plasmon does not become ambiguous due to the presence of damping.[20]

For the case where the surface-plasmon wavelengths of interest are much shorter than the counterelectrode thickness, $ql \gg 1$, Eq. (2.2) has the approximate solution

$$\omega(q) = \omega_p\left\{\tanh\left(q\frac{d}{2}\right)\Big/\left[1+\tanh\left(q\frac{d}{2}\right)\right]\right\}^{1/2}. \qquad (2.3)$$

Equation (2.2) has another solution which lies at higher frequencies and represents a radiative surface plasmon which can couple to real photons.[21] This second solution is thus drastically altered at small q when retardation is included, but it does not respond effectively at optical frequencies in the microstructures considered and is not of interest here. A third solution given by $\epsilon = -1$ corresponds to a surface plasmon at the counterelectrode-vacuum interface. This lies at a single q-independent frequency $\omega_p/\sqrt{2}$ due to neglect of retardation. The effect of including retardation for the nonradiative surface plasmon, Eq. (2.3), would only be to push the $\omega(q)$ curve down slightly at small q to ensure that it always lies below the light line $\omega = qc$. In this case Eq. (2.3) is changed to

$$\omega(q) = \omega_p\left\{\tanh\gamma\left(q\frac{d}{2}\right)\Big/\left[\Gamma + \tanh\left(\gamma q\frac{d}{2}\right)\right]\right\}^{1/2}, \quad (2.4)$$

where

$$\gamma = [1 - (\omega/qc)^2]^{1/2} \quad (2.5)$$

and

$$\Gamma\gamma = [1 + (\omega_p^2 - \omega^2)/(qc)^2]^{1/2}. \quad (2.6)$$

Then we see that $\omega(q) \to qc$ as $q \to 0$ so that the long wavelength surface plasmon becomes less localized near the interface and begins to resemble a photon. Note that if the wavelength is much larger than the oxide thickness, $qd/2 \ll 1$, yet still much shorter than the counterelectrode, Eq. (2.3) reduces to

$$\omega(q) = \omega_p(qd/2)^{1/2}. \quad (2.7)$$

In another limit, we examine Eq. (2.2) in the case that the wavelengths are comparable to the counterelectrode thickness, $ql \sim 1$. If the wavelengths are also much larger than the oxide thickness, $qd/2 \ll 1$, we find the approximate solution

$$\omega(q) = \omega_p[qd \tanh ql/(1 + \tanh ql)]^{1/2} \quad (2.8)$$

which reduces to Eq. (2.7) when $ql \gg 1$. In the limit $ql \ll 1$, this becomes linear in q,

$$\omega(q) = \omega_p q(dl)^{1/2}. \quad (2.9)$$

The plasmon field is now able to reach across the top electrode and induce surface charges on the outer surface. The character of the modes becomes less that of a surface wave concentrated at one boundary, as in Eq. (2.7), and begins to resemble an excitation spread across the junction. As $q \to 0$, the dispersion relation approaches qc due to retardation effects. The effect of a finite counterelectrode thickness is to hasten this changeover at small q from the $\sim q^{1/2}$ dispersion characteristic of a two-dimensional mode to the linear dispersion characteristic of a one-dimensional mode.

The form of the surface plasmons in these different limits gives insight into the modes which are allowed when the planar counterelectrode is modified as shown in Figs. 1(b)–1(d). For these cases, the translational invariance along the surface of the counterelectrode is broken causing the surface-plasmon dependence on the wave vector to be changed. The physical picture of the microstructure counterelectrode operating as a wave guide beyond the cutoff suggests itself. For the case in Fig. 1(b) of a spherical particle, we look for a mode confined beneath the particle. The size of a cavity formed in this way will depend on both a and d, and for our estimate we characterize the size by the distance out from the particle bottom to the point where it has curved up a distance d, or $L \simeq (2ad)^{1/2}$. Here we have assumed $d/a \ll 1$. The wave vectors are then set by $q \sim L^{-1}$ and, by Eq. (2.7), the frequencies are of order

$$\omega_1 = \omega_p(d/8a)^{1/4} = \omega_{sp}(d/2a)^{1/4}. \quad (2.10)$$

In this picture, a set of discrete resonant frequencies appears below the limiting surface plasmon frequency ω_{sp} with the lowest given approximately by Eq. (2.10). For oxide spacing $d = 20$ Å and particle radius $a = 150$ Å, $(d/2a)^{1/4} \simeq 0.51$. The resonances will move toward higher frequencies as particle size decreases varying as $a^{-1/4}$, for the free-electron metal considered here. Indeed, we would expect that as the surface plasmons are required to be confined over smaller distances, more high-frequency modes are required to form a wave packet of corresponding extent under the microstructure. Modes confined beneath the particle are sensitive to the local curvature near the surface.

For the case in Fig. 1(c) of a cylindrical slab, a surface plasmon localized across the width $2a$ of the cylinder would have wave vectors set by $q \sim a^{-1}$. First, when the cylinder thickness is comparable to the width, $l/a \sim 1$, the frequencies are set by Eq. (2.8) to be of order

$$\omega_2 = \alpha\,\omega_{sp}(d/a)^{1/2}, \quad (2.11)$$

where α is a constant of order unity. These modes are more sensitive to microstructure size, varying as $a^{-1/2}$, than the particle modes of Eq. (2.10).

If the slab were extremely thin, $l/a \ll 1$, the frequencies are given by Eq. (2.9) to be of order

$$\omega_3 = \omega_{sp}(2dl)^{1/2}/a. \quad (2.12)$$

Here the allowed wavelengths of the localized plasmon are much larger than the slab thickness, and the geometric mean of the oxide and slab thickness enters the relation rather than just the oxide thickness. With $l = d = 20$ Å and $a = 150$ Å, the coefficient has the value $(2dl)^{1/2}/a \simeq 0.19$. This compares with $(d/a)^{1/2} \simeq 0.37$ from Eq. (2.11) so that the thick-slab mode frequency ω_2 is almost twice that of the thin-slab mode frequency ω_3. Of course the localized surface plasmons will be able to lose energy to electronic excitations in the metals and thus each of the levels will be broadened. In addition, the estimates in Eqs. (2.11) and (2.12) must be further corrected by factors of order unity. For example, the slab modes would, to lowest order, have a wave vector set by $q \simeq \eta/a$ where η is the lowest zero of $J_0'(x)$. The potential of the lowest mode is described approximately by $J_0(qr)$ and is described physically by requiring the current associated with the mode to be approximately zero at the sides of the slab. These types of considerations are included for the complete calculation presented in Sec. III.

A type of mode in which the fields are extended across the thickness l of the slab is expected to be more easily excited in the thin cylindrical rod ($l/a \gg 1$) of Fig. 1(d). The thin rod also has advantages with respect to the emission of radiation. The surface-plasmon solutions, Eqs. (2.7)–(2.9), correspond to waves which propagate along the interfaces as $\exp(i\vec{q}\cdot\vec{r})$ and decay in the direction normal to the interfaces as $\exp(-qz)$. These solutions therefore cannot be used directly to make an estimate for a plasmon solution propagating along the length of the rod, i.e., normal to the oxide interface. However, in an attempt to make such a correspondence we substitute $q \to iq$ in Eq. (2.8):

$$\omega^2(q) \simeq -\omega_p^2 qd \tan ql\,. \tag{2.13}$$

In the next section we will obtain an approximate solution for the fields excited in the thin rod microstructure in order to get some feeling for the characteristics of localized modes. We will see that the relation Eq. (2.13) is approximately valid and that the wave vector is set by $q \sim l^{-1}$. There is an additional weak dependence of q on the radius a of the rod provided by the propagation of the excitation along the sides of the rod which have a curvature of $1/a$. The localized plasmons confined along the length of the thin rod have frequencies which vary roughly as $\omega_p(d/l)^{1/2}$.

The values of the localized surface-plasmon resonant frequencies and their dependence on the junction geometry are quite sensitive to the microstructure under consideration and the type of mode being examined. A great deal of control over the localized mode frequency spectrum is thus available by the choice of microstructure geometry. The metal used for the microstructure and substrate is also important because this determines the overall scale ω_p of the mode frequencies. If different metals for microstructure and substrate are used, a reduced-average plasma frequency $\overline{\omega}_p$ sets the scale. An oxide dielectric constant with a value greater than unity will lower the frequencies due to the additional polarization it creates. The damping of the localized surface plasmons, set by the imaginary part of the metal dielectric functions, is also important to the character of the frequency spectrum.

B. Thin rod microstructures

In order to obtain an approximate form for the surface plasmons confined along the length of the thin rod of Fig. 1(d), we describe the metal of the rod by the dielectric function $\epsilon(\omega)$, the oxide layer by the dielectric constant ϵ_0, and treat the substrate metal as a perfect conductor. The assumption of a perfect conductor allows us to include the substrate by way of an image rod antenna. Under these conditions the problem resembles a dielectric dipole antenna of length $2(l+d)$ including an excitation gap of width $2d$ filled with dielectric ϵ_0 at the center. Solutions of Eq. (2.1) for the fields in this structure are easily found if we require the current to vanish at the ends of the rod, $z=\pm l$. As discussed in Appendix A, the tunneling excitation of the microstructure plasmons is well described by a localized antisymmetric charge distribution,

$$\rho(\vec{x},\omega) = \frac{Q(\omega)}{\pi a^2}\left[\delta(z-d) - \delta(z+d)\right]\Theta(a-r)\,. \tag{2.14}$$

Here the center of the oxide gap is chosen to be the $z=0$ plane and $Q(\omega)$ describes the frequency spectrum of the tunneling charge fluctuations. The solution for the potential of Eq. (2.1) is then found for the lowest mode, in the region $r<a$, to be

$$\psi(q,z) = \frac{4Q(\omega)I_0(qr)}{qa^2[\epsilon_0 - \epsilon(\omega)\tan ql\,\tan qd]} \times \begin{cases} \operatorname{sgn}(z)\dfrac{\tan qd}{\cos ql}\cos q(|z|-l-d), & d<|z|<l \\ \dfrac{\sin qz}{\cos qd}, & |z|<d \end{cases} \tag{2.15}$$

where $I_0(qr)$ is a modified Bessel function. Here the conditions that ψ be continuous and that the discontinuity in $-\epsilon d\psi/dz$ equal 4π times the surface charge density at $z=\pm d$ have been imposed.

Notice that in the special case of a free-electron metal $\epsilon(\omega) = 1-(\omega_p/\omega)^2 \simeq -(\omega_p/\omega)^2$, $\epsilon_0 = 1$, and $qd \ll 1$ the potential Eq. (2.15) has resonances at frequencies given by Eq. (2.13). We see this approximate form as a general feature characteristic of a plasmon mode excited across a gap of width d into a structure of thickness l. However, for the case of a finite microstructure such as the rod, there are additional boundary conditions which further restrict the allowed values of q. At the sides of the rod, $r=a$, ψ and $-\epsilon\partial\psi/\partial r$ are required to be continuous. If we impose these matching conditions in the approximation that we neglect effects at the end of the rod and distortions of the field at the side gap, we find the following relation between ω and q:

$$\epsilon(\omega)I_1(qa)K_0(qa)+K_1(qa)I_0(qa)=0\,, \tag{2.16}$$

where $K_n(x)$ is a modified Bessel function of the second type. For a free-electron metal the dispersion relation Eq. (2.16) can be written

$$\omega=\omega_{sp}[2qaI_1(qa)K_0(qa)]^{1/2}\,, \tag{2.17}$$

where $\omega_{sp}=\omega_p/\sqrt{2}$. For plasmon wavelengths much shorter than the rod radius $qa\gg 1$, the rod curvature should appear small, and indeed we note from Eq. (2.17) that $\omega\simeq\omega_{sp}$ in this limit. In the opposite limit of very long wavelengths $qa\ll 1$, the modes should only be sensitive to the direction along the length of the rod, and we find approximately

$$\omega=\omega_{sp}qa[-\ln(qa/2)-\gamma]^{1/2}\equiv vq\,, \tag{2.18}$$

where Euler's constant has the value $\gamma=0.577$. In this regime the logarithmic term will be slowly varying, and the square-root factor will be of order unity. Then for long wavelengths, v is nearly constant, and the dispersion is linear in q.

The localized surface-plasmon potential is approximately given, for the lowest mode, by Eq. (2.15) where the allowed values of q obey Eq. (2.16). The dipole moment induced by these fields will be directed approximately along the length of the rod. This can be found using the relation

$$p(\omega)=\frac{\epsilon(\omega)-1}{4\pi}\int dV\,E_z\,. \tag{2.19}$$

Performing the integral for these fields over the rod above the conducting substrate we find

$$p(\omega)=\frac{Q(\omega)}{q}\tan qd\,\frac{[(1-\epsilon)\cos qd+(\epsilon-\epsilon_0)\cos ql]}{(\epsilon_0\cos ql-\epsilon\sin ql\tan qd)}\,. \tag{2.20}$$

Note that this is a complex quantity because the dielectric function for a real material has a dissipative part. Owing to our approximation that the currents vanish at the end of the rod, the dipole solution for the lowest plasmon mode is expected to resonate for an allowed value of q near $\pi/2l$. However, we see from Eq. (2.13) that the wave vector is required to be slightly above this value, $q=(1+\delta)\pi/2l$, to find real frequencies. The actual value of δ is determined by the curvature of the rod by Eq. (2.16). For $q=\pi/2l$, Eq. (2.18) gives approximately

$$\omega\simeq\frac{\pi}{2}\,\omega_{sp}\left(\frac{a}{l}\right). \tag{2.21}$$

We are interested in exciting the localized plasmon resonances at optical frequencies, say $\omega=2.0$ eV. This puts a constraint on the shape of the rod l/a. For a rod mode of a free-electron material such as Al where $\omega_{sp}\simeq 11.0$ eV, Eq. (2.21) would require $l/a\simeq 10$. For an Au rod where ω_{sp} [in this case defined by $\epsilon(\omega_{sp})=-\epsilon_0$] lies at the upper end of the free-electron conduction region at 2.4 eV, this would require $l/a\simeq 2$. This does not represent an extremely thin rod, and we see that very thin Au rods are more easily excited in the infrared. The constraints are actually not as tight as Eq. (2.18) would lead us to believe, and we can obtain optical resonances in Au from Eqs. (2.20) and (2.16) with $l/a\simeq 7-3$. To obtain these solutions, we use optically measured complex dielectric functions for Au,[22] take the oxide material to have a dielectric constant $\epsilon_0=3$ corresponding to Al_2O_3, and use the $qa\ll 1$ limit of Eq. (2.16). In the optical regime the quantity $[-\ln(qa/2)-\gamma]^{1/2}$ remains within a few percent of unity. The magnitude of the dipole, Eq. (2.20), is plotted as a function of frequency in Fig. 2 for several values of l/a. This represents, for each value of l/a, the lowest localized mode, and we see that it consists of a broadened resonance peak lying below ω_{sp}. The resonance frequency decreases as l becomes larger and the plasmon becomes less localized. With d/l fixed we expect the frequency to vary as a/l by Eq. (2.21). With a/l fixed we expect it to vary as $(d/l)^{1/2}$ from Eq. (2.13) for free-electron materials. However the magnitude of the dipole at resonance increases with l. In addition, the strong damping due to interband transitions quenches the amplitude of

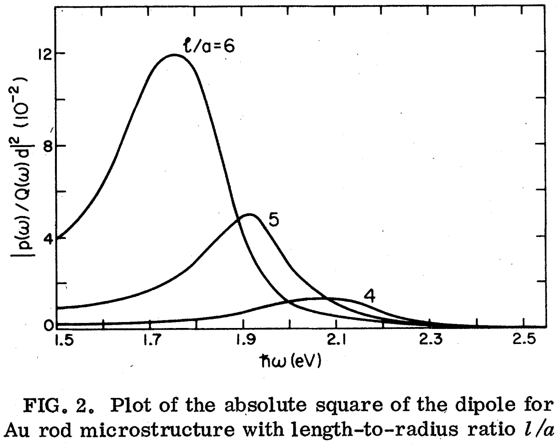

FIG. 2. Plot of the absolute square of the dipole for a Au rod microstructure with length-to-radius ratio l/a. The oxide has dielectric constant $\epsilon_0=3$ and thickness $d=0.2a$.

the induced dipole as ω increases above 2 eV. We see from Eq. (2.20) that for q near $\pi/2l$, $p(\omega)$ becomes proportional to $Q(\omega)l$ as the oscillating currents fill up the rod.

The approximate solution, Eqs. (2.20) and (2.16), neglects some features. The currents are not identically zero at the end of the dielectric rods. The cavity waves would then be required to fit into some effective length $l+\Delta l$. The rod ends and the gap have been ignored in deriving the relation Eq. (2.16). The dispersion relation will have some correction for the finite length of the rod, and the fields in the gap will also be altered. The details would be given by the solution to a full boundary-value problem. The approximations leading to Eq. (2.20) are in fact equivalent to replacing the rod microstructure above a tunnel junction by the equivalent circuit shown in Fig. 3 in the limit $qa \ll 1$, $\epsilon_0 = 1$. A current generator $I(\omega) = -i\omega Q(\omega)$ will cause current to flow along the rod. A capacitance $C = \pi a^2/8\pi d$ in parallel with the impedance $Z(\omega)$ of this generator requires a current given by

$$I(\omega,z) = I(\omega)\,\frac{\sin q(l-z)}{\sin ql + (i\omega/4\pi\sigma)\cos ql/qd}\,, \qquad (2.22)$$

where σ is the conductivity of the metal and the currents are required to vanish at $z = l$. The dipole of this antenna is found from

$$p(\omega) = \frac{i}{\omega}\int_0^l dz\, I(\omega,z)\,. \qquad (2.23)$$

Using the relation $4\pi\sigma/i\omega = 1-\epsilon$, we obtain a dipole equal to Eq. (2.20) in the limit $qd \ll 1$, $\epsilon_0 = 1$.

The equivalent circuit approximation describes the general features of surface plasmons localized by thin rods on tunnel junctions with good conducting substrates. Free-standing 120-Å-diameter Au wires have already been fabricated.[23]

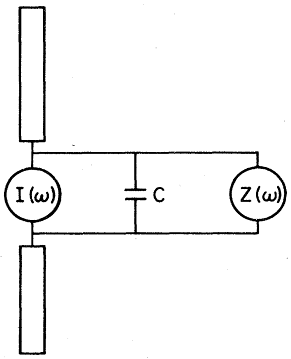

FIG. 3. Equivalent circuit for the approximate rod microstructure solution.

Such wires with lengths of about 400 Å are expected to contain optical localized plasmons when excited by electron tunneling. If the rods are spaced so that they do not strongly couple with each other, the radiation spectrum from these localized modes will be dominated by the structure shown in Fig. 2. Note that the tunneling current has a very local spatial coherence so that the current driving different rods is incoherent. The equivalent circuit solution for the rod is presented in this section to illustrate the dependence of the excited spectrum of a microstructure on the parameters of the problem. A more complete microstructure solution, for the case of the spherical particle in Fig. 1(b), including the radiation spectrum is presented in the following sections.

III. SPHERICAL PARTICLE MICROSTRUCTURES

A. Solution for a single particle

For the calculation of surface plasmons localized by a spherical particle on a tunnel junction, we use a model based on the geometry of Fig. 4. These modes are mostly confined underneath the particle near the oxide layer and do not extend into the space surrounding the particle. Therefore it is a good approximation to allow the material of the entire space to be described by the dielectric constant of the oxide layer, $\epsilon^{(0)}$. This is only in error for the limit $d/a \gg 1$ which is not realized in junction structures of interest here. The estimate in Sec. II A indicates that the surface plasmons would be confined by the particle to a region of order $L = (2ad)^{1/2}$. For $d = 20$ Å and $a = 150$ Å, $L \sim 80$ Å and we can neglect retardation for particles of this size. This estimate was based on a modification

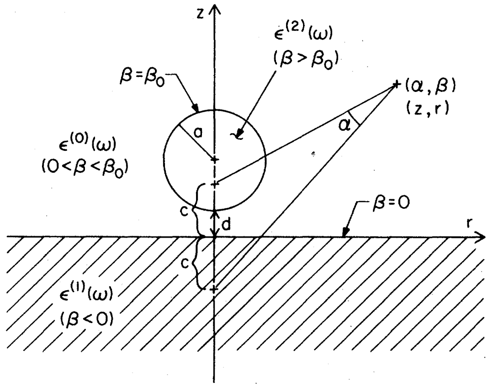

FIG. 4. Geometry of a spherical metal particle above a metal film used to calculate localized modes. Cylindrical coordinates (z, r) and bispherical coordinates (α, β) are indicated.

of the smooth junction surface-plasmon solutions to account for the geometry of the microstructure. For the detailed calculations here, we do not use eigenfunctions of the extended surface plasmons but use different ones in which the microstructure modifications can be handled exactly.

We need to solve Eq. (2.1), where $\epsilon(\vec{x}, \omega)$ takes on the value $\epsilon^{(1)}$ in the substrate, $\epsilon^{(0)}$ in the oxide, and $\epsilon^{(2)}$ in the particle. As discussed in Appendix A, a localized antisymmetric charge distribution ρ gives a good description of the tunneling excitation by

$$\rho(\vec{x}, \omega) = Q(\omega)[\delta(z-d) - \delta(z)]\frac{\delta(r)}{2\pi r}. \tag{3.1}$$

Here the bottom of the oxide layer is chosen to be the $z=0$ plane and as before $\rho(\omega)$ describes the frequency spectrum of the tunneling charge fluctuations. Equation (2.1) can be solved in our geometry by using bispherical coordinates[24] α, β, ϕ shown in Fig. 4 in which

$$r = \frac{c\sin\alpha}{\cosh\beta - \cos\alpha}, \quad z = \frac{c\sinh\beta}{\cosh\beta - \cos\alpha}, \tag{3.2}$$

where $c = (d^2 + zad)^{1/2}$. Note that $c \simeq (2ad)^{1/2}$ for $d/a \ll 1$ so that these coordinates have a measure of the characteristic localization length built into them. A surface of constant β, say β_0, represents a sphere with center at a distance $(a+d)$ above the $z=0$ plane, where

$$\cosh\beta_0 = 1 + \frac{d}{a}. \tag{3.3}$$

For $d/a \ll 1$, $\beta_0 \simeq (2d/a)^{1/2}$. The coordinate α is an angular coordinate which sweeps over the β spheres by taking on values between 0 and π. For the case of cylindrical symmetry, the potential ψ will be independent of the azimuthal coordinate.

Laplace's equation can be separated in these coordinates apart from a factor $F(\alpha, \beta) = [2(\cosh\beta - \cos\alpha)]^{1/2}$. The cylindrically symmetric potentials in the three regions take the form

$$\psi^{(0)}(\alpha,\beta) = F(\alpha,\beta)\sum_{n=0}^{\infty}\{A_n \exp[-(n+\tfrac{1}{2})(\beta-\beta_0)] + B_n \exp[(n+\tfrac{1}{2})(\beta-\beta_0)]\}P_n(\mu), \quad 0<\beta<\beta_0 \tag{3.4}$$

$$\psi^{(1)}(\alpha,\beta) = F(\alpha,\beta)\sum_{n=0}^{\infty}\{A_n \exp[(n+\tfrac{1}{2})\beta_0] + B_n \exp[-(n+\tfrac{1}{2})\beta_0]\}\exp[(n+\tfrac{1}{2})\beta]P_n(\mu), \quad \beta<0 \tag{3.5}$$

$$\psi^{(2)}(\alpha,\beta) = F(\alpha,\beta)\sum_{n=0}^{\infty}(A_n+B_n)\exp[-(n+\tfrac{1}{2})(\beta-\beta_0)]P_n(\mu), \quad \beta>\beta_0 \tag{3.6}$$

where $\mu \equiv \cos\alpha$. Here the coefficients have been chosen to make the potentials continuous at the boundaries $\beta=0$ and $\beta=\beta_0$. A second boundary condition requires that the discontinuity in the normal component in $\vec{D}$ is equal to 4π times the surface charge density at the interfaces. The surface charge densities corresponding to Eq. (3.1) written in bispherical coordinates are

$$\sigma^{(1)}(\alpha) = [-2Q(\omega)/\pi c^2]\delta(\cos\alpha+1), \quad \beta=0 \tag{3.7}$$

$$\sigma^{(2)}(\alpha) = [2Q(\omega)/\pi c^2][(\cosh\beta_0+1)/2]^2\delta(\cos\alpha+1), \quad \beta=\beta_0 \tag{3.8}$$

where the δ function can be written

$$\delta(\mu+1) = \sum_{n=0}^{\infty}(-1)^n(n+\tfrac{1}{2})P_n(\mu). \tag{3.9}$$

We apply the second boundary condition on the $z=0$ plane ($\beta=0$) and obtain the relation

$$A_n = \Gamma_n + \frac{\epsilon^{(0)}-\epsilon^{(1)}}{\epsilon^{(0)}+\epsilon^{(1)}}B_n\exp[-(2n+1)\beta_0] \tag{3.10}$$

with

$$\Gamma_n = -2(-1)^n\frac{Q(\omega)/c}{\epsilon^{(0)}+\epsilon^{(1)}}\exp[-(n+\tfrac{1}{2})\beta_0]. \tag{3.11}$$

Applications of the boundary condition on the sphere ($\beta=\beta_0$) produces, after using Eq. (3.10) and the recursion relation of the Legendre polynomials, the equation

$$-U_n\bar{B}_n + V_n\bar{B}_{n-1} + W_n\bar{B}_{n+1} = S_n, \tag{3.12}$$

where

$$\overline{B}_n = B_n/[Q(\omega)/c]\,, \tag{3.13}$$

$$U_n = -g\,\big[(\chi^{(2)}\{1+\chi^{(1)}\exp[-(2n+1)\beta_0]\})\sinh\beta_0 + (2n+1)\{1-\chi^{(1)}\chi^{(2)}\exp[-(2n+1)\beta_0]\}\cosh\beta_0\big]\,, \tag{3.14}$$

$$V_n = -gn\{1-\chi^{(1)}\chi^{(2)}\exp[-(2n-1)\beta_0]\}\,, \tag{3.15}$$

$$W_n = -g(n+1)\{1-\chi^{(1)}\chi^{(2)}\exp[-(2n+3)\beta_0]\}\,, \tag{3.16}$$

$$g = (\epsilon^{(0)}+\epsilon^{(1)})(\epsilon^{(0)}+\epsilon^{(2)})\,, \tag{3.17}$$

$$\begin{aligned} S_n = 2(-1)^n\big((\epsilon^{(0)}+\epsilon^{(1)})2(2n+1)[(\cosh\beta_0+1)/2]^{3/2} + (\epsilon^{(0)}-\epsilon^{(1)})\{[\sinh\beta_0-(2n+1)\cosh\beta_0]\exp[-(n+\tfrac{1}{2})\beta_0] \\ - n\exp[-(n-\tfrac{1}{2})\beta_0] - (n+1)\exp[-(n+\tfrac{3}{2})\beta_0]\}\big)\,, \end{aligned} \tag{3.18}$$

$$\chi^{(i)} = (\epsilon^{(0)}-\epsilon^{(i)})/(\epsilon^{(0)}+\epsilon^{(i)})\,. \tag{3.19}$$

Equation (3.12) is an inhomogeneous second-order linear difference equation for the coefficients B_n of the nth mode of the potential ψ. Solutions to equations of this form can be found in terms of infinitely continued fractions by applying a Green's function technique for difference equations.[25] However, a direct numerical approach has been found to be more convenient here for evaluating the coefficients. Equation (3.12) is also equivalent to a tridiagonal matrix equation of infinite order. If a cutoff is introduced to reduce the equation to a finite matrix relation, the solutions are found to have good convergence properties as a function of the cutoff.

For particles with diameter a few hundred angstroms, the excitation spectrum at optical frequencies is dominated by the dipole moment of the modes. An expression for the dipole can be found from a multipole expansion of Eq. (3.4). The bispherical surface $\beta=0$ is a sphere of infinite radius resting on the $z=0$ plane. Large distances from the origin lie on the $\beta=0$ surface at $\alpha=0$. Equation (3.2) shows that at infinity z approaches $2c/\beta$. Using this we expand at large distances above the particle. After using Eq. (3.10), we can identify the dipole term as

$$p(\omega) = Q(\omega)c\,\frac{8\epsilon^{(1)}(\omega)}{\epsilon^{(0)}+\epsilon^{(1)}(\omega)} \times \sum_{n=0}^{\infty}(n+\tfrac{1}{2})\overline{B}_n\exp[-(n+\tfrac{1}{2})\beta_0]\,. \tag{3.20}$$

The monopole term can also be identified and, since this should vanish identically, leads to the condition

$$2\epsilon^{(0)}\sum_{n=0}^{\infty}\overline{B}_n\exp[-(n+\tfrac{1}{2})\beta_0] = 1\,. \tag{3.21}$$

Alternatively Eq. (3.21) can be derived, without assuming the monopole vanishes, by writing down the β_0 matching condition for $\vec{D}$ and integrating it over the surface of the sphere. This sum rule adjusts the coefficients so as to keep the system neutral and is extremely useful for checking the numerical cutoff procedure when calculating the coefficients $\overline{B}_n$.

Numerical solutions for the dipole show that each $\overline{B}_n$ has a resonance peak centered at a certain frequency. To examine some of the features of these resonant modes, we consider the simpler case where the particle is perfectly conducting, $\epsilon^{(2)}\to-\infty$. In this case the complicated boundary condition on the surface of the sphere can be avoided and exact solutions for the $\overline{B}_n$ can be found.[9] The $\overline{B}_n$ have resonant denominators $\Delta_n(\omega)$ given by

$$\Delta_n(\omega) = \epsilon^{(0)}\cosh(n+\tfrac{1}{2})\beta_0 + \epsilon^{(1)}(\omega)\sinh(n+\tfrac{1}{2})\beta_0\,. \tag{3.22}$$

At optical frequencies, the complex substrate dielectric $\epsilon^{(1)}(\omega)=\epsilon_1(\omega)+i\epsilon_2(\omega)$ can have a negative real part. The dipole can then have a resonance at frequencies determined approximately by

$$\epsilon_1(\omega) = -\epsilon^{(0)}/\tanh(n+\tfrac{1}{2})\beta_0\,. \tag{3.23}$$

For $\epsilon_1(\omega)=1-(\omega_p/\omega)^2$, a free-electron material, this condition becomes

$$\omega = \omega_p\{\tanh(n+\tfrac{1}{2})\beta_0/[\epsilon^{(0)}+\tanh(n+\tfrac{1}{2})\beta_0]\}^{1/2}\,. \tag{3.24}$$

For the lowest mode, $n=0$, we see the correspondence of the localized mode frequency Eq. (3.24) with $\beta_0\simeq(2d/a)^{1/2}$ and the extended surface-plasmon frequency Eq. (2.3) with the wave vector set by $q\sim(2ad)^{-1/2}$. To lowest order, when $d/a\ll1$ and $\epsilon^{(0)}=1$, Eq. (3.24) reduces to our previous estimate Eq. (2.10) within a factor of order unity. The $d/a\ll1$ limit should best represent surface plasmons confined beneath the particle and will closely correspond to the perfectly conducting particle approximation where the fields do not penetrate the particle. In the general case, the fields of the localized plasmon always penetrate the particle to some extent and begin to reach across the particle when $d/a\gtrsim1$. Also, if the particle dielectric responds within the frequency range of interest, proper treatment of the particle becomes crucial for the solution of the modes even for small values of d/a. Below we will consider Au particles, which can excite surface plasmons at optical frequencies, and Al film substrates which do not. The factor $1/(\epsilon^{(0)}+\epsilon^{(1)})$ in Eq. (3.20) represents the excitation of a surface plasmon at the substrate-oxide interface and will not contribute structure in the case of Al.

Surface plasmons localized by spherical particles are represented by an infinite set of discrete levels lying below the planar surface-plasmon frequency of the particle material. The imaginary parts of the dielectric functions cause these levels to broaden and possibly overlap. The positions of the levels are determined by the ratio of oxide spacing to particle radius as measured by $\beta_0 \simeq (2d/a)^{1/2}$. If the oxide spacing is given, then β_0 is a measure of the size of the spherical particle. However, for $d/a \lesssim 1$, the confined fields probe mostly the underside of the particle, and therefore only its geometry in this region should affect the solutions. Therefore the parameter β_0 will describe the curvature of the particle near the substrate even if it is not spherical. The curvature becomes flatter as β_0 decreases. Modes confined by particles of arbitrary shape can be described by the spherical particle model as long as the fields probe only the local curvature.

We consider Au particles on an Al substrate with Al_2O_3 as oxide. We take $\epsilon^{(0)}=3$ for the oxide[26] and use optically measured data for the Al and Au dielectric functions.[22] The dipole coefficients $\overline{B}_n$ were calculated from Eq. (3.12) for several particle curvatures using the numerical cutoff technique. The calculated $\overline{B}_n$ are complex numbers which tend to alternate in sign with n reflecting the alternating charge source distributions Eqs. (3.7) and (3.8). The magnitude of the calculated dipole moments is shown in Fig. 5 as a function of frequency. As shown by Eq. (3.20), the higher-order modes are suppressed exponentially in the dipole, but the number of modes which contributes depends on the size of the particle. High-order modes have a less-localized character and more of these are necessary to describe the fields as the confinement area spreads out. Therefore, more terms are needed in the dipole sum as the size of the particle increases or the local curvature decreases. The localized mode equations describe confinement very well but are less effective as the modes spread out. For $\beta_0=0.3$, a cutoff on the matrix equation for the $\overline{B}_n$'s at $n=25$ and summing 15 terms satisfies the sum rule Eq. (3.21) to about 5%. A cutoff at $n=30$ and summing 20 terms satisfies it to about 1%. The value of the imaginary part of the dielectric function of the particle material ϵ_2 determines the damping of each mode and can thus also effect the magnitude of the $\overline{B}_n$'s. If ϵ_2 decreases sufficiently fast with frequency, some of the higher-order modes can in fact be stronger than the lowest few modes.

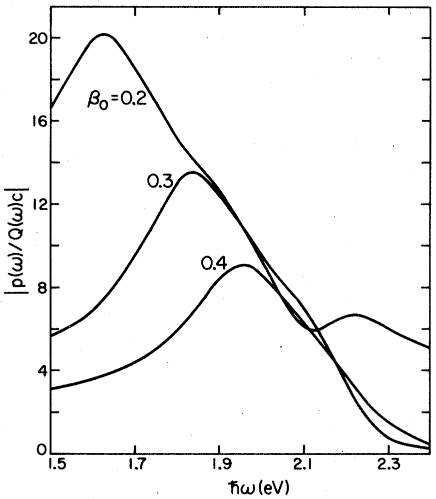

FIG. 5. Plot of the magnitude of the dipole moment for a Au particle above an Al substrate. Here $\epsilon^{(0)}=3$ and $\beta_0 \simeq (2d/a)^{1/2}$ gives a measure of the curvature of the particle near the surface.

The particle resonant frequencies decrease with increasing particle size as we argued earlier. We note also that the size of the dipole increases with particle size. These features were shared qualitatively with the modes of the thin rod in Fig. 2. The $\beta_0=0.4$ plot is a sum of the 20 lowest modes which lie in the region from $\hbar\omega \simeq 1.95$ eV to the surface-plasmon limiting frequency of the Al_2O_3-Au interface at $\hbar\omega_{sp} \simeq 2.4$ eV. The modes are close enough together to overlap and form a broad peak centered near $\hbar\omega=1.95$ eV. For the $\beta_0=0.3$ case, the contributing modes are spread over an extra electron volt in energy and the resulting separation between the lowest few modes and the other higher-order modes shows up as a slight structure near $\hbar\omega=2.1$ eV. The modes for the $\beta_0=0.2$ case are spread out enough to actually show a small second peak near $\hbar\omega=2.2$ eV. The onset of interband damping[27] in Au occurs above $\hbar\omega \simeq 2$ eV and helps to further suppress the localized plasmon resonances.

The α and β components of the electric field are obtained from

$$\left.\begin{matrix} E_\alpha \\ E_\beta \end{matrix}\right\} = -\frac{1}{c}(\cosh\beta - \cos\alpha)\times\left\{\begin{matrix} \dfrac{\partial\psi}{\partial\alpha} \\ \dfrac{\partial\psi}{\partial\beta} \end{matrix}\right. . \qquad (3.25)$$

Cylindrical coordinate components E_z and E_r are found by applying the chain rule with these equations. We use these to calculate the fields for the Au particle calculation. In Fig. 6, we show the envelope of the magnitude of the z component of the electric field along the z and r directions under the particle for $\hbar\omega = 1.85$ eV and $\beta_0 = 0.3$. We see in Fig. 6(b) that the field has a 90% falloff within a distance of $(2ad)^{1/2}$ from a point directly beneath the particle in agreement with the estimate of Sec. II A. This estimate should be applicable here since $\beta_0 = 0.3$ corresponds to $d/a \simeq 0.045$.

B. Surface distribution of particles

The dipole moment for surface plasmons confined by a single particle on a tunnel junction was calculated in the previous section. We now deal with a distribution of microstructures over the junction surface in order to calculate the radiation from such a system. The particles are assumed to be spaced far enough apart so that interactions between particles do not affect the calculated moments. From the shot-noise picture of tunneling discussed in Appendix A, we do not expect any correlation between the excitation of different particles. The particles are then expected to radiate incoherently, and we can simply multiply the expression for the tunneling current power spectrum given by Eq. (A5) by the number of particles. This has the effect of changing R_0 to the total junction resistance and hence V/R_0 to the total current.

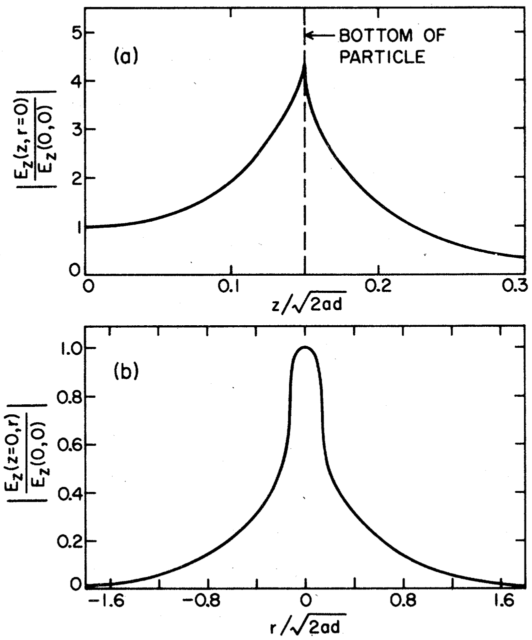

FIG. 6. Plot of the envelope of the z component of the electric field beneath the Au particle along the z and r axes. Here $\beta_0 = 0.3$, $\hbar\omega = 1.85$ eV, and $\epsilon^{(0)} = 3$.

The localized mode solutions neglected retardation, and thus the radiated fields are not part of our solution. These can be found by treating the fluctuating microstructure dipole as a radiating current source above a substrate. In this situation a reciprocity relation is useful because it treats in a natural way the question of properly including near-field effects due to the existence of the substrate. Let the current of a single dipole be $\vec{J}_p(\vec{x}_p)$ and the field radiated to a distant observation point be $\vec{E}_p(\vec{x}_0)$. Suppose a point source $\vec{J}_0(\vec{x}_0) = \hat{\theta}\delta(\vec{x} - \vec{x}_0)$ is located at the observation point, and it radiates a field $\vec{E}_0(\vec{x}_p)$ to the position of the dipole, as shown in Fig. 7. Then the reciprocity theorem states[28]

$$E_p(r,\theta) = \int dV\,\vec{E}_0 \cdot \vec{J}_p \,. \tag{3.26}$$

Thus the problem of calculating the field radiated by J_p is related to the simpler problem of finding the field at the dipole from a hypothetical point source at the observation point. This theorem is based on the physical fact that the transmitting and receiving radiation patterns of an antenna are the same. The radiated field $\vec{E}_p$ will only have a $\hat{\theta}$ component because the source $\vec{J}_p$ from the calculated localized modes points only in the z direction. Thus it can only emit p-polarized radiation. This is a consequence of confining attention to current fluctuations normal to the junction. Due to asymmetries in particle shape and the local particle distribution, a small component of s-polarized radiation may also be emitted.

Since the point source radiates plane waves and the dimensions of the microstructure are much smaller than the observation distance, Eq. (3.26) is approximated by

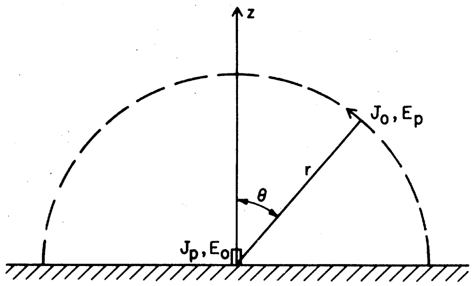

FIG. 7. Schematic of the geometry used to calculate radiation from a microstructure using the reciprocity theorem. Here J_p and E_p are the current and radiated field of the microstructure, while J_0 and E_0 are the current and radiated field of a distant hypothetical point source.

$$E_p(r,\theta) \simeq -iE_z(0)\omega p(\omega)\,. \qquad (3.27)$$

The field $E_z(0)$ is the z component of the p-polarized plane wave emitted by the point source and located under the particle. The form for this is well known,

$$E_z(0) = \frac{-i\omega}{c^2}\frac{e^{ikr}}{r}\sin\theta g(\omega,\theta)\,. \qquad (3.28)$$

The factor $g(\omega,\theta)$ is included to account for the scattering of the incoming plane wave by the layer of particles and the substrate. If we could neglect the effect of the particles on the plane waves, it would equal $[1+\Gamma(\omega,\theta)]$, where $\Gamma(\omega,\theta)$ is the familiar Fresnel reflection coefficient for p-polarized waves on the oxide-substrate system. In general the distribution of microstructures cannot be neglected in the function $g(\omega,\theta)$ and is important for the angular distribution of the radiation and for the absolute magnitude of the intensity spectrum.

Equation (3.27) is used to calculate the power radiated per unit angle $\Delta\Omega$ and per unit frequency $\Delta\omega$ by the usual methods of electromagnetism. We find

$$\mathcal{I}(\theta,\omega)\Delta\omega\Delta\Omega = \frac{|p(\omega)|^2}{8\pi c^3}\omega^4\sin^2\theta\,|g(\omega,\theta)|^2\Delta\omega\Delta\Omega\,. \qquad (3.29)$$

If the power has been time averaged, the current source for the dipole will be $C(\omega)$ of Eq. (A5) and Eq. (3.29) becomes

$$\mathcal{I}(\theta,\omega)\Delta\omega\Delta\Omega = IV\frac{\alpha}{4}\left(\frac{c}{\lambda_V}\right)^2\left(\frac{\hbar\omega}{eV}\right)^2\left(\frac{p(\omega)}{Q(\omega)c}\right)^2\left(1-\frac{\hbar\omega}{eV}\right)\sin^2\theta\,|g(\theta,\omega)|^2\frac{\hbar\Delta\omega}{eV}\Delta\Omega\,. \qquad (3.30)$$

Here $c=(d^2+2ad)^{1/2}$ is the bispherical confinement length, IV is the dc power dissipated in the biased tunnel junction, $\lambda_V \equiv \hbar c/eV$ is the wavelength corresponding to the tunneling current cutoff, and the tunneling power spectrum restricts the frequencies to $0<\hbar\omega \leqslant eV$. The fine-structure constant α appears as a scale because we are expressing the confinement length in units of λ_V and the photon energy in eV. The factor $(c\hbar\omega/\lambda_V eV)^2$ is the usual $(kL)^2$ part of the dipole radiation formula.

The total emitted power can be calculated from Eq. (3.30),

$$P=\int_0^\infty d\omega\int d\Omega\,\mathcal{I}(\theta,\omega)\,. \qquad (3.31)$$

Then an overall efficiency ϵ for the conversion of dc energy into radiation is given by

$$\epsilon = P/IV\,. \qquad (3.32)$$

We use the dipole calculated for the Au-Al_2O_3-Al system and shown in Fig. 5 to get an order-of-magnitude estimate. For an oxide spacing of $d=20$ Å, $\beta_0=0.3$ corresponds to a confinement length of $(2ad)^{1/2}\simeq 130$ Å and $\beta_0=0.4$ to $(2ad)^{1/2}\simeq 100$ Å. For a bias voltage of $V=2.5$ V and a surface factor $g_\omega(\theta)=2$, we find $\epsilon\simeq 1.5\times 10^{-4}$ at $\beta_0=0.3$ and $\epsilon\simeq 3.5\times 10^{-5}$ at $\beta_0=0.4$. The coupling improves as the particle size increases. We consider the shape of the emission spectrum in relation to experimental evidence after discussing a model for the surface distribution of spherical particles.

The surface distribution function $g(\theta,\omega)$ can be found by calculating the z component of the E field under the particles from an incident plane wave at angle θ. The problem of plane-wave reflection from a surface covered with metal particles is quite difficult. A simple approximation to this problem which may capture some of the general features is to treat the distribution of particles as a layer of material with an effective dielectric constant. If the inhomogeneities in a dielectric material are on a sufficiently large scale so that in each part of space the behavior of the material is controlled by macroscopic constitutive equations, we need only find a reasonable way to average over the statistical variations of the material. The averaging is particularly simple if the inhomogeneities are not large enough and dense enough that we must consider fluctuations of the field throughout the material. The treatment of dielectric materials under these conditions has been closely connected with the development of the molecular field concept. Many extensions of these theories have been developed in recent years.[29]

Here we will use a version based on the Clausius-Mossotti relation with explicit account taken of the plasmon resonant structure associated with the particles. For a random distribution of isotropic dipoles within a medium of dielectric constant ϵ_0, the Clausius-Mossotti relation for the effective dielectric function of the system is

$$\tilde{\epsilon}(\omega)=\epsilon_0\left(1+\frac{4\pi n\alpha}{1-\frac{4}{3}\pi n\alpha}\right)\,. \qquad (3.33)$$

Here n is the volume density of the dipoles and α is the polarizability of a dipole by the local field within a spherical hole surrounding the dipole. If the distribution is not too dense, we expect that a dipole finds itself, on the average, surrounded by other dipoles in what would be a good approximation to a spherical hole.

We propose to use the polarizability of the spherical particle-substrate system in Eq. (3.33) and obtain an expression for the effective dielectric function of the layer of particles. The general features of Eq. (3.33) can first be illustrated using a simpler example, that of isolated spheres made of dielectric material $\epsilon(\omega)$. An isolated sphere of radius R has polarizability given by

$$\alpha = R^3 \frac{\epsilon(\omega) - \epsilon_0}{\epsilon(\omega) + 2\epsilon_0} . \tag{3.34}$$

We consider a free-electron metal and $\epsilon_0 = 1$. An isolated sphere thus has a plasmon resonance near the frequency $\omega_r = \omega_p/\sqrt{3}$. In this case Eq. (3.33) can be rewritten as

$$\tilde{\epsilon}(\omega) = (\omega_L^2 - \omega^2 - i\omega/\tau)/(\omega_T^2 - \omega^2 - i\omega/\tau), \tag{3.35}$$

where $\omega_L^2 = \omega_p^2(1+2f)/3$, $\omega_T^2 = \omega_p^2(1-f)/3$, and f is the fraction of total volume occupied by the spheres. This effective dielectric function is similar in form to that of a crystal with two atoms per unit cell and transverse and longitudinal optical phonon frequencies ω_T and ω_L. $\mathrm{Re}\,\tilde{\epsilon}(\omega) < 0$ for $\omega_T < \omega < \omega_L$, that is, between the pole ω_T and the zero ω_L of $\tilde{\epsilon}(\omega)$. As f increases and the spheres begin to fill up the bulk of the medium, ω_T approaches zero. As f approaches zero, ω_T reaches the value of the isolated sphere resonance frequency ω_r. Our mean-field-type approximation is, however, expected to be valid only for rather small f. We schematically show the form of $\tilde{\epsilon}(\omega)$ in Fig. 8.

The case of spherical particles above a substrate is worked out in the same way. The needed polarizability is actually a tensor and the incoming plane wave could induce several components of polarization in the particles. The most important component is assumed to be normal to the substrate. We then apply a uniform electric field normal to the junction surface and work out the induced dipole of the spherical particle-substrate system. The potentials can be written in the form of Eqs. (3.4)–(3.6) with the addition of extra terms to represent the electric field in the absence of the particle. These extra terms are

$$\Delta\psi^{(0)}(\alpha,\beta) = -D_0 z/\epsilon^{(0)}, \quad 0 < \beta < \beta_0 \tag{3.36}$$

$$\Delta\psi^{(1)}(\alpha,\beta) = -D_0 z/\epsilon^{(2)}, \quad \beta < 0$$

$$\Delta\psi^{(2)}(\alpha,\beta) = -D_0 z/\epsilon^{(0)}, \quad \beta > \beta_0. \tag{3.37}$$

Here D_0 is the uniform displacement normal to the substrate. We can then carry out the process of matching the boundary conditions as in Sec. III A, except here there is no external tunneling charge. There is a condition identical to Eq. (3.10) except with $\Gamma_n = 0$. Using this, one finds a set of equations similar to Eq. (3.12) from which the coefficients $\overline{B}_n = B_n/(2cD_0/\epsilon^{(0)})$ of the dipole can be obtained. The dipole is given by Eq. (3.20) except with $Q(\omega)c$ replaced by $(2D_0c^3/\epsilon^{(0)})$. Due to the absence of external charge for this case the sum rule is given by

$$\sum_{n=0}^{\infty} \overline{B}_n \exp[-(n+\tfrac{1}{2})\beta_0] = 0. \tag{3.38}$$

The polarizability is found from $\alpha(\omega) = p(\omega)/(D_0/\epsilon^{(0)})$. In the special case of a perfectly conducting particle, the $\overline{B}_n$ can be found exactly and they are found to have the same resonance denominators as the coefficients for the tunneling resonance given by Eq. (3.22).

We calculate the polarizability for Au particles, Al substrate, $\epsilon^{(0)} = 3$ and $\beta_0 = 0.3$. With these parameters we can combine the results with the dipole calculation from Sec. III A. The calculated polarizability has a resonance near $\hbar\omega = 1.85$ eV which is the same as found for the tunnel-excited $\beta_0 = 0.3$ particle in Fig. 5. In Figs. 9(a) and 9(b), we plot the real and imaginary parts of $\tilde{\epsilon}(\omega)$ computed from Eq. (3.33) using the calculated polarizability. We look for qualitative features similar to those found in the simpler free-electron isolated sphere case of Eq. (3.35) and Fig. 8. The value of ω_L, where $\mathrm{Re}\,\tilde{\epsilon}(\omega)$ goes through zero, is seen to increase with f as expected from the isolated sphere example. The large peak in $\mathrm{Im}\,\tilde{\epsilon}(\omega)$, corresponding to ω_T, moves towards zero as f increases also as expected. However, the structure in Fig. 9 is more complicated due to the use of experimentally measured dielectric functions and the more complex nature of the particle-substrate

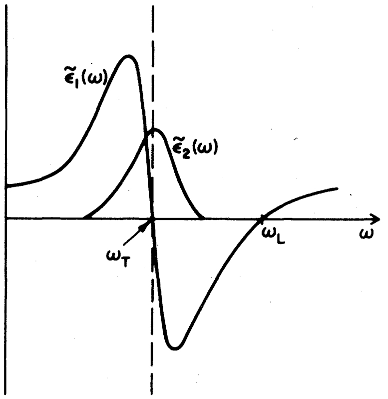

FIG. 8. Schematic of the real and imaginary parts of the dielectric function of an effective medium layer of free-electron metal spheres in vacuum.

polarizability. This model of an effective dielectric layer of spherical particle-substrate plasmon resonators can now be applied to calculate features of the radiation spectrum.

C. Radiation spectrum of particles

For purposes of calculating the surface distribution function $g(\omega, \theta)$, we consider a system consisting of an infinitely thick Al substrate, an Al_2O_3 layer of thickness d, a layer of thickness l described by the effective dielectric function $\tilde{\epsilon}(\omega)$ of particle-substrate resonances, and vacuum. The z component of the electric field beneath the effective dielectric layer from a p-polarized incident plane wave of unit amplitude can be identified with $g(\omega, \theta)$ in this model. This is straightforward to evaluate and is given by Eq. (B1) in Appendix B. The thickness of the effective dielectric layer is taken to be equal to the diameter of the particles. For a distribution of different sized particles, we might use some average or weighted thickness. With oxide thickness $d = 20$ Å, then $\beta_0 = 0.3$ corresponds to $a \simeq 250$ Å. According to the spherical particle model, when $d/a \ll 1$, β_0 is a measure of the curvature of the bottom of the particle, and the modes are insensitive to the actual thickness normal to the junction. Then for a description of an actual distribution of particles on a tunnel junction, the thickness of the spherical particle corresponding to β_0 and the effective dielectric layer thickness need not be the same. Here to illustrate general features we take them to be equal.

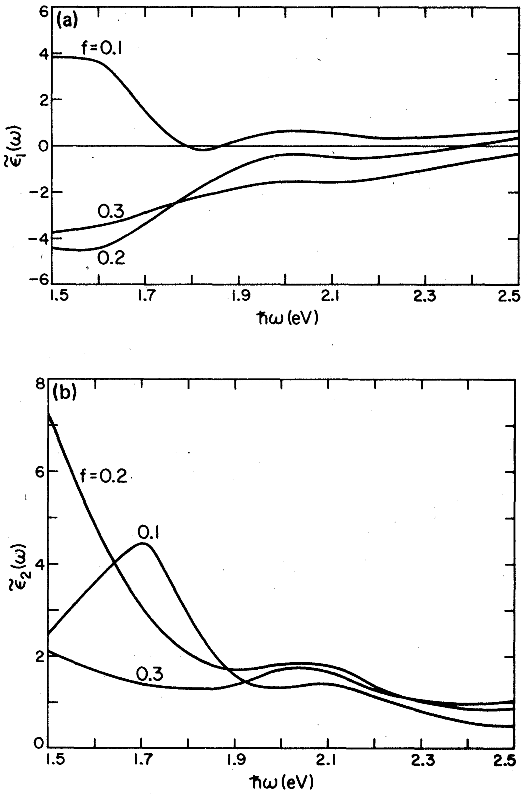

FIG. 9. (a) Plot of the real part of the dielectric function of an effective medium layer of Au particle–Al substrate resonators at several values of the particle volume fraction f. Here $\beta_0 = 0.3$ and the surrounding medium is vacuum. (b) Plot of the imaginary part of the dielectric function corresponding to Fig. 9(a).

Using the effective dielectric model for the surface distribution and the spherical particle model for localized surface plasmons, we compare the results of the calculated radiation emission, Eq. (3.30), with experimental data reported by Hansma and Broida[7] and Adams, Wyss, and Hansma.[8] They observed light emission from tunnel junctions in which Au particles have been evaporated onto an oxidized Al substrate. Estimates from electron micrographs show a typical Au particle to be of order 300 Å in diameter. Agglomeration of particles into clusters was noted along with some isolated particles. Particle coverage on the surface was of order 10%.

The observed emission intensity as a function of photon energy took the form of a broad spectrum which, for bias voltages $\lesssim 2$ volts, was characterized by an upper linear frequency cutoff given by $\omega_{co} = eV/\hbar$. However, for larger voltages, a strong, broad peak appears in the spectrum near 1.9 eV and was independent of the bias voltage as the voltage was raised. The observed light remained red at higher voltages until the junction burned out. This feature suggests that localized surface plasmons are playing a role, and this interpretation was taken by Adams *et al.*[8] based on comparisons with the spherical particle theory.[9]

The efficiencies of the experimental junctions were measured to be within the range $(0.5-5) \times 10^{-5}$. Our estimated efficiencies from Sec. III B were within this range for $\beta_0 = 0.3-0.4$. From the calculated dipoles of localized plasmons in Fig. 5 we see that $\beta_0 = 0.3-0.4$ correspond to resonant peaks near 1.9 eV in agreement with the observed spectrum. For an oxide spacing of $d = 20$ Å, these β_0 values correspond to a particle radius between 250 and 440 Å. Recall that the spherical particle model interprets β_0 as a measure of the curvature of the bottom of the particles. This curvature is difficult to obtain from electron micrographs. The distributions of particles on the experimental junctions were quite complex; however we estimate that a typical radius of curvature near the oxide was of order $a \sim 300$ Å.

The observed light emission was found to be partially polarized. At $\theta = 0°$ the s and p components of the intensity were found to be equal and nonzero. At $\theta = 90^\circ$ both components were essentially zero. For other angles the p-polarized component dominated. In Fig. 10(a) we plot the shape of the calculated angular dependence $|g(\omega, \theta)|^2 \sin^2\theta$ of the radiation intensity, Eq. (3.30), for $\hbar\omega = 2.0$ eV, $\beta_0 = 0.3$ and a 10% coverage of particles. In the absence of the substrate $|g(\omega, \theta)|^2 = 1$ and the angular pattern would consist of a lobe peaked at $\theta = 90^\circ$ from the z axis. The presence of the substrate below the particle has the effect of lifting the peak from $\theta = 90^\circ$ to an angle above the substrate. Since our model confines attention to the dominant z-directed current, our spectrum is entirely p polarized. However, our intensity vanishes at $\theta = 0^\circ$ in contrast to the observed p component of Adams *et al.*[8] shown in Fig. 10(b). Adams *et al.* note that the difference between the p and s components produced a lobe peaked near $\theta = 55^\circ$ similar to the localized plasmon prediction. A physical interpretation is that dipole oscillations in the plane of the junction can contribute both s- and p-polarized light while oscillations perpendicular to the junction can only contribute p polarization. The difference between p and s is the excess p polarization from perpendicular current oscillations expected in the localized plasmon theory.

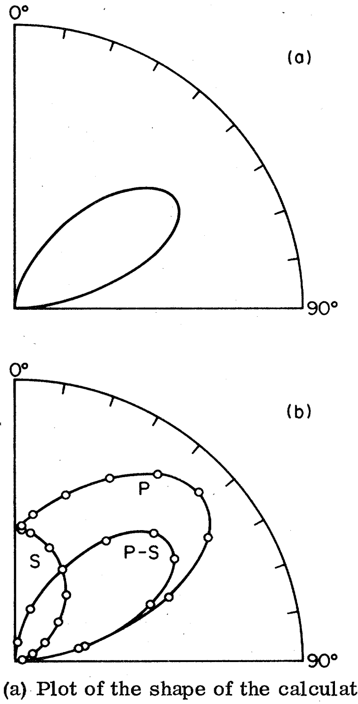

FIG. 10. (a) Plot of the shape of the calculated angular distribution of the Au particle intensity at $\hbar\omega = 2.0$ eV. Here $\beta_0 = 0.3$ and $\epsilon^{(0)} = 3$. (b) Plot of the experimental angular distribution for the Au particle junction of Ref. 8. The bias viltage is 2.3 volts.

This interpretation finds further support from the calculations of Laks and Mills.[18] They have worked out a detailed theory of light emission from slightly roughened tunnel junctions using the perturbation methods of surface roughness mentioned in Sec. I. There is no large-scale "geometrical" roughness in this theory which can localize surface plasmons. Instead a Gaussian distribution of random surface roughness plays the role of coupling the surface plasmons to the radiation field. Surface plasmons radiate most efficiently when the wave vector is of order $q \sim a^{-1}$, where a is the transverse correlation length of the random roughness. Their results agree well with the experiments of Lambe and McCarthy[2,3] on small-scale roughness junctions. Laks and Mills also point out that their theory should be relevant to the junctions used by Adams *et al.*[18] Small amplitude roughness is also expected to play a role in these junctions. Indeed, Laks and Mills find roughly equal contributions from s and p polarization. Their calculated angular distributions for both components are virtually identical to the s component measured by Adams *et al.*[8] and shown in Fig. 10(b). Therefore, Adams *et al.* seem to be observing s- and p-polarized radiation from plasmons coupled by small amplitude roughness along with a p-polarized component from plasmons localized by large-scale roughness. The localized modes may also emit a small s-polarized component.[30]

The localized plasmons show striking directional properties. The position of the calculated lobe peak at $\theta \simeq 55^\circ$ is not sensitive to the particle coverage for $f = 0.1-0.5$. The lobe becomes slightly narrower as f increases. The calculated angular dependence agrees well with experiment in shape and peak position although it must be emphasized that the effective medium treatment of the particles is not a complete description of this part of the problem. The angular dependence calculated by ignoring the particles and using the reflection coefficient for a flat surface to calculate $g(\omega, \theta)$ results in a lobe at $\theta \simeq 70^\circ$ below the normal. Some consideration of the layer of particles is evidently needed to raise the lobe above the substrate to the observed value.

In Fig. 11(a) we plot the shape of the calculated frequency dependence of the radiation intensity, Eq. (3.30), for $\theta = 60^\circ$, $\beta_0 = 0.3$, and a 10% coverage of particles. This shows the localized plasmon resonance characteristic of a $\beta_0 = 0.3$ particle near $\hbar\omega = 1.9$ eV. As discussed in Sec. III B, the effective dielectric layer has a characteristic resonant absorption frequency ω_T which lies below the resonant frequency of the localized modes by an amount which depends on the particle coverage

f. This effective medium absorption provides additional suppression of the dipole emission at low frequencies. The factor $|g(\omega, \theta)|^2$ is frequency dependent but does not affect the strong resonant structure of the localized surface plasmons. It runs from ~ 0.3 at $\hbar\omega = 1.5$ eV to ~ 3.3 at $\hbar\omega = 1.9$ eV. Damping of the surface plasmons by interband transitions in Au for the $\hbar\omega \gtrsim 2$ eV provides further suppression above the peak.[27]

The measured spectrum of Adams *et al.*[18] for the $p-s$ polarization component is shown in Fig. 11(b), along with the smaller s component. The excess p polarization measured by the $p-s$ component is, again, expected to correspond to localized plasmon emission. The observed resonant peak is broader than the calculated one, but the calculated intensity shown in Fig. 11(a) corresponds to particles of only one size. A weighted distribution of particle sizes would broaden the spectrum. The observed s-polarized component shows only a very weak peak near $\hbar\omega = 1.9$ eV indicating that small-scale roughness is not dominant here. We believe this is strong evidence that localized surface plasmons are excited in these junctions. In Fig. 12 we plot the calculated spectrum for several bias voltages. Here we see excitation of the localized plasmon as inelastic tunneling channels open up. Note the linear cutoff due to the tunneling power spectrum at $V = 1.9$ volts. The relative spacings of the curves are comparable to those observed by Hansma and Broida.[7]

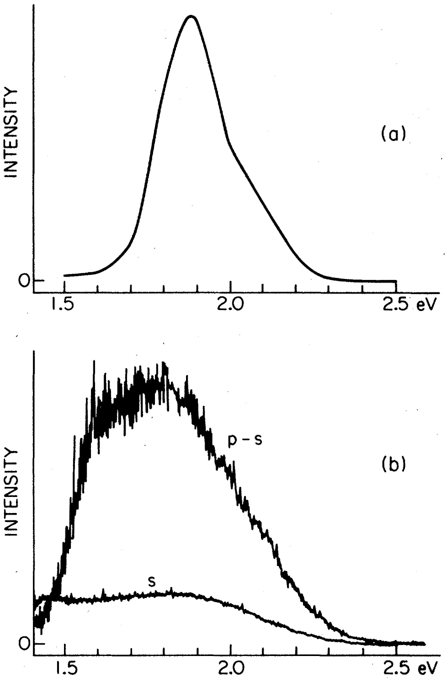

FIG. 11. (a) Plot of the calculated Au particle intensity spectrum at $\theta = 60°$ and at a bias voltage of 2.7 volts. Here $\beta_0 = 0.3$, $\epsilon^{(0)} = 3$, and $f = 0.1$. (b) Plot of the measure intensity spectrum for the Au particle junction of Ref. 8. Here $\theta = 60°$ and the bias voltage is 2.7 volts.

Laks and Mills[18] find that if they choose a transverse correlation length for their model random surface roughness on the order of 50 Å, the surface plasmons can radiate efficiently in the visible spectrum and produce a peak in the spectrum near $\hbar\omega = 1.9$ eV. Thus surface plasmons coupled to small-amplitude roughness can produce spectral features similar to surface plasmons localized by microstructures if the transverse correlation length is comparable to the localized mode confinement region. However, the angular distribution of the radiation calculated by Laks and Mills is most intense along the normal to the film and decreases smoothly to zero as the emission angle increases. This is in distinct contrast with the lobe structure of the angular distribution of the p-polarized radiation, Fig. 10(a), obtained from the model discussed in this section. In addition, the surface roughness model gives about an equal admixture of s- and p-polarized radiation. From electron micrographs it is clear that the present geometries consist of both particles and agglomerate regions so that the observed radiation should contain both types of radiation.

The radiation spectrum should depend on the density of the particles distributed over the surface of the junction in two ways. The tunneling current can excite more particles as more are added, and the current will then increase as f. Secondly, we expect the layer of particles to act more and more like a solid metal film as particles are added and the emitted radiation to be screened. For particle densities low enough to leave the localized plasmon dipole unaffected, the intensity depend-

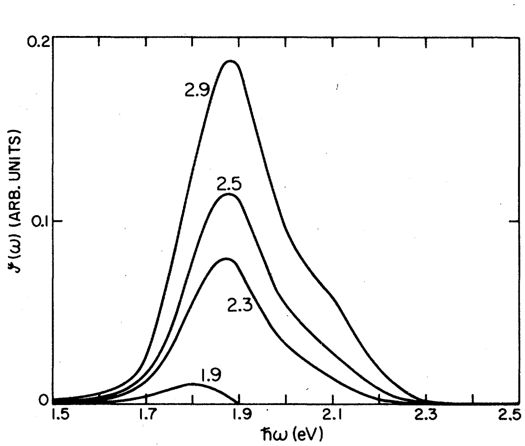

FIG. 12. Plot of the calculated Au particle intensity spectrum for several bias voltages. Here $\theta = 60°$, $\beta_0 = 0.3$, $\epsilon^{(0)} = 3$, and $f = 0.1$.

ence on f will be

$$\mathscr{I}(f) = f\,|g(f)|^2, \tag{3.39}$$

where the function $g(\omega, \theta)$ depends on f. Within the effective medium model for the particle layer we find, at the peak frequency, that the slope of $\mathscr{I}(f)$ decreases slightly for $f = 0.1 - 0.4$ indicating that the intensity may in fact be starting to saturate with density. However no actual saturation or optimum density is seen for the small values of f allowed by the effective medium theory. In addition, the structure of the localized plasmons will begin to alter when particles approach one another within a distance of about one radius. The details of this phenomenon must be handled by a more complete theory of the surface distribution. A related phenomenon has been observed by McCarthy and Lambe,[3] where light emission from roughened junctions saturated as the roughness was increased. Laks and Mills[18,19] have examined this within their perturbation theory and have found a trend towards such a saturation.

As noted, for the present evaporated particle tunnel junctions, the intensity contains contributions from both localized plasmons and small-scale roughness. It would be interesting to study more controlled situations using, for instance, precisely microfabricated structures in which the different-order plasmon modes could be displayed. At least a partial separation of modes can be obtained using a Ag spherical particle. The calculated dipole is shown in Fig. 13, and we note the contrast to the case of Au. Here we see a peak near $\hbar\omega = 1.9$ eV and a second larger peak near $\hbar\omega = 2.6$ eV. The imaginary part of the dielectric function of Ag decreases in this region so as to make several of the higher modes more important than the first few. In addition, the use of alternate materials could prove interesting.

ACKNOWLEDGMENTS

We have had many helpful discussions with Professor P. K. Hansma, Dr. A. Adams, and Dr. J. C. Wyss, Professor D. L. Mills and Dr. B. Laks, and Professor B. Mühlschlegel. We want to thank Professor P. K. Hansma, Dr. A. Adams, and Dr. J. C. Wyss for allowing us to reproduce their data from Ref. 8. This research was supported in part by the National Science Foundation.

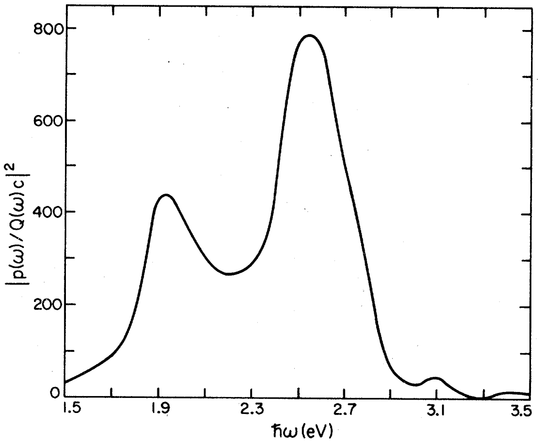

FIG. 13. Plot of the absolute square of the dipole for a Ag particle above an Al substrate. Here $\beta_0 = 0.25$ and $\epsilon^{(0)} = 3$.

APPENDIX A: TUNNELING CURRENT FLUCTUATIONS

A dc bias voltage V across a tunnel junction causes a dc current to flow across the oxide barrier. It is the time dependent fluctuations about this current, $\vec{J}(\vec{x}, t)$, that drive the surface plasmons. Davis,[31] in his treatment of surface-plasmon excitation in tunnel junctions, has argued that these current fluctuations are spatially extended structures in the direction parallel to the junction interfaces. However, because of the effect of impurity, phonon and interface scattering, it is more likely that a localized picture is relevant for realistic tunnel junctions. The transverse correlation length L of the current fluctuations will have an upper limit set by the electron mean-free path. For the cases of interest in this paper there will be an additional limit set by the spatial extent of the microstructures. We argue that the fluctuations have the character of shot noise and that only the frequency spectrum is of importance for tunneling into microstructures.

The time-averaged power absorbed by the surface plasmons is given by the classical electromagnetism formula

$$\begin{aligned} P &= -\frac{1}{2T}\int_{-T}^{T} dt \int d^3x\, \vec{E}(\vec{x}, t)\cdot\vec{J}(\vec{x}, t) = -\frac{1}{2T}\int_{-T}^{T} dt \int d^3x \int_{-\infty}^{t} dt' \int d^3x'\, K(\vec{x}-\vec{x}', t-t')\langle J(\vec{x}', t')\, J(\vec{x}, t)\rangle \\ &= -\int d^3x \int d^3x'\, |f(\vec{x}-\vec{x}')|^2 \int_0^{\infty} d\tau\, K(\vec{x}-\vec{x}', \tau) \int_{-\infty}^{\infty} d\omega\, e^{-i\omega\tau}\, \frac{1}{2\pi}\, \frac{|I(\omega)|^2}{2T}\,. \end{aligned} \tag{A1}$$

Here K is some appropriate kernal relating the plasmon field to the current, and we have dropped all dyadic notation for illustrative purposes. Our tunneling currents must be quantum-mechanical objects so we introduce the necessary averaging brackets. The current correlation is assumed to factor into a spatial part represented by $f(\vec{x}-\vec{x}')$ and a time-dependent part $\langle I(t')I(t)\rangle$. The Fourier transform of the time-dependent part of the current correlation $C(\omega)$ is the tunneling-current power spectrum

$$C(\omega)=\frac{1}{2\pi}\,\frac{|I(\omega)|^2}{2T}\,. \tag{A2}$$

This is easily evaluated within the tunneling Hamiltonian formalism[32,33] and is given at zero temperature by

$$C(\omega)=2(e/\hbar)^2|T|^2N^2(0)(eV-\hbar\omega). \tag{A3}$$

Here $|T|$ is a suitable average of the tunneling matrix element, $N(\epsilon)$ is the density of states, and the frequencies are restricted by $0<\hbar\omega<eV$. The dc tunneling current can be evaluated in a similar manner with the result

$$I(V)=2(e/\hbar)^2|T|^2N^2(0)2\pi V\equiv V/R_0, \tag{A4}$$

where R_0 is the dc junction resistance. If the tunneling matrix elements for these two processes were the same, we could then write

$$C(\omega)=\frac{eV}{2\pi R_0}\left(1-\frac{\hbar\omega}{eV}\right). \tag{A5}$$

In fact, the matrix element will be different in the inelastic case due to the spatial dependence of the wave functions in the z direction. In Eq. (A5) R_0 would be replaced by a larger effective resistance. However, Eq. (A5) as it stands gives the dominant frequency dependence of the tunneling-current fluctuations and leads to a useful estimate of the radiation spectrum by Eq. (3.30).

The low-energy nonradiative branch of surface plasmons which we deal with in this paper and modify using microstructures is excited by the antisymmetric part of the tunneling charge distribution[21] so that we use

$$\rho(\vec{x},\omega)=\sigma(r,\omega)[\delta(z-d)-\delta(z)] \tag{A6}$$

as the plasmon driving source in Eq. (2.1). Here d is the oxide barrier thickness. Our arguments for a localized current fluctuation imply that the r dependence of $\sigma(r,\omega)$ will not be relevant here. The frequency dependence will be given by Eq. (A5).

APPENDIX B: SURFACE DISTRIBUTION FUNCTION

In Sec. III C, the z component of the electric field beneath the effective dielectric layer of a p-polarized incident plane wave of unit amplitude was identified as the surface distribution function $g(\omega,\theta)$. This can be computed in a straightforward manner by matching fields at the interfaces of vacuum, effective medium, oxide, and substrate. The result is

$$g(\omega,\theta)=\left\{E_2^+\exp\left[-\left(i\frac{\omega}{c}n_2\frac{d}{2}\cos\theta_2\right)\right]+E_2^-\exp\left(i\frac{\omega}{c}n_2\frac{d}{2}\cos\theta_2\right)\right\}\sin\theta_2\,, \tag{B1}$$

where

$$E_2^+=T_{32}\exp\left\{-\left[i\frac{\omega}{c}\left(l+\frac{d}{2}\right)\right]\right\}\times\left[1+R_{32}F_{24}\exp\left(2i\frac{\omega}{c}n_2l\cos\theta_2\right)\right]^{-1}, \tag{B2}$$

$$E_2^-=E_2^+F_{24}\exp\left[-\left(2i\frac{\omega}{c}n_2\frac{d}{2}\cos\theta_2\right)\right], \tag{B3}$$

$$F_{24}=\left[R_{20}+R_{04}\exp\left(4i\frac{\omega}{c}n_0\frac{d}{2}\cos\theta_0\right)\right]\times\left[1+R_{20}R_{04}\exp\left(4i\frac{\omega}{c}n_0\frac{d}{2}\cos\theta_0\right)\right]^{-1}, \tag{B4}$$

$$R_{jk}=(n_k\cos\theta_j-n_j\cos\theta_k)(n_k\cos\theta_j+n_j\cos\theta_k)^{-1}, \tag{B5}$$

$$T_{jk}=2n_j\cos\theta_j(n_k\cos\theta_j+n_j\cos\theta_k)^{-1}, \tag{B6}$$

$$\cos\theta_j=[1-(n_3/n_j)^2\sin^2\theta_3]^{1/2}, \tag{B7}$$

$$n_j=[\epsilon^{(j)}(\omega)]^{1/2}. \tag{B8}$$

Here region (0) is the oxide, (1) is the metal substrate, (2) is the effective medium layer, and (3) is the vacuum region above the junction. Thus θ_3 is equal to the angle of incidence θ.

---

*Present address: National Bureau of Standards, Washington, DC 20234.

[1] Proceedings of the NSF Workshop on Opportunities for Microstructures Science, Engineering and Technology in Cooperation with the NRC Panel on Thin Film Microstructures Science and Technology, 1978, Arlie, Virginia (unpublished); Phys. Today 30 (1979).

[2] J. Lambe and S. L. McCarthy, Phys. Rev. Lett. 37, 923 (1976).

[3] S. L. McCarthy and J. Lambe, Appl. Phys. Lett. 30,

427 (1977).

[4] S. L. McCarthy and J. Lambe, Appl. Phys. Lett. 33, 858 (1978).

[5] E. Kröger and E. Kretschmann, Z. Phys. 237, 1 (1970); A. A. Maradudin and D. L. Mills, Phys. Rev. B 11, 1392 (1975).

[6] D. L. Mills, Phys. Rev. B 12, 4036 (1975).

[7] P. K. Hansma and H. P. Broida, Appl. Phys. Lett. 32, 545 (1978).

[8] A. Adams, J. C. Wyss, and P. K. Hansma, Phys. Rev. Lett. 42, 912 (1979).

[9] R. W. Rendell, D. J. Scalapino, and B. Mühlschlegel, Phys. Rev. Lett. 41, 1746 (1978).

[10] R. K. Jain, S. Wagner, and D. H. Olson, Appl. Phys. Lett. 32, 62 (1978).

[11] R. H. Ritchie, E. T. Arakawa, J. J. Cowan, and R. N. Hamm, Phys. Rev. Lett. 21, 1530 (1968).

[12] E. Kretschmann, T. L. Ferrell, and J. C. Ashley, Phys. Rev. Lett. 42, 1312 (1979); R. Kotz, H. J. Lewerenz, and E. Kretschmann, Phys. Lett. 70A, 452 (1979); T. S. Rahman and A. A. Maradudin, Phys. Rev. B 21, 2137 (1980).

[13] S. O. Sari, D. K. Cohen, and K. D. Scherkoske, Phys. Rev. B 21, 2162 (1980).

[14] K. Ohtaka, H. Miyazaki, and A. A. Lucas, Phys. Rev. B 21, 467 (1980).

[15] J. E. Rowe, C. V. Shank, D. A. Zwemer, and C. A. Murray, Phys. Rev. Lett. 44, 1770 (1980).

[16] H. Metiu, private communication.

[17] D. A. Weitz, T. J. Gramila, A. Z. Genack, and J. I. Gersten, Phys. Rev. Lett. 45, 355 (1980).

[18] B. Laks and D. L. Mills, Phys. Rev. B 20, 4962 (1979).

[19] B. Laks and D. L. Mills, Phys. Rev. B 21, 5175 (1980).

[20] R. W. Alexander, G. S. Kovener, and R. J. Bell, Phys. Rev. Lett. 32, 154 (1974).

[21] R. H. Ritchie, Surf. Sci. 34, 1 (1973).

[22] H. J. Hageman, W. Gudat, and C. Kunz, J. Opt. Soc. Am. 65, 742 (1975); DESY Report No. SR-74/7 (unpublished).

[23] A. N. Broers, J. Cuoma, J. Harper, W. Molzen, R. R. Laibowitz, and R. Pomerants, in Proceedings of the International Congress on Electron Microscopy, Toronto, 1978, edited by J. M. Sturgess, Vol. III, p. 43 (unpublished).

[24] P. M. Morse and H. Feshbach, *Methods of Theoretical Physics* (McGraw-Hill, New York, 1953), Vol. II., p. 1298.

[25] J. D. Love, Q. J. Mech. Appl. Math. 28, 449 (1975); L. M. Milne-Thomson, *The Calculus of Finite Differences* (MacMillan, London, 1960), pp. 531–533.

[26] L. Holland, *Vacuum Deposition of Thin Films* (Chapman and Hall, London, 1970), pp. 351–352.

[27] M. Guerrisi and R. Rosei, Phys. Rev. B 12, 557 (1975).

[28] W. L. Weeks, *Antenna Engineering* (McGraw-Hill, New York, 1968).

[29] *Electrical Transport and Optical Properties of Inhomogeneous Media (Ohio State University, 1977)*, Proceedings of the First Conference on the Electrical Transport and Optical Properties of Inhomogeneous Media, edited by J. C. Garland and D. B. Tanner (AIP, New York, 1978).

[30] We note that Laks and Mills also present a calculation of radiation by direct coupling of current fluctuations in a smooth junction counterelectrode. This shows directional p-polarized angular lobes. If this mechanism is also operating in the more complex geometry of the particle junctions, it may affect the magnitude of the calculated intensities.

[31] L. C. Davis, Phys. Rev. B 16, 2482 (1977).

[32] J. Bardeen, Phys. Rev. Lett. 6, 57 (1961).

[33] D. Rogovin and D. J. Scalapino, Ann. Phys. (N.Y.) 86, 1 (1974).